Monthly Notices
of the
ROYAL ASTRONOMICAL SOCIETY

MNRAS **435,** 2903–2917 (2013) doi:10.1093/mnras/stt1489
Advance Access publication 2013 September 4

Galaxy And Mass Assembly: resolving the role of environment in galaxy evolution

S. Brough,[1⋆] S. Croom,[2] R. Sharp,[3] A. M. Hopkins,[1] E. N. Taylor,[2,4] I. K. Baldry,[5] M. L. P. Gunawardhana,[2,1] J. Liske,[6] P. Norberg,[7] A. S. G. Robotham,[8,9] A. E. Bauer,[1] J. Bland-Hawthorn,[2] M. Colless,[1] C. Foster,[10] L. S. Kelvin,[8,9,11] M. A. Lara-Lopez,[1] Á. R. López-Sánchez,[1,12] J. Loveday,[13] M. Owers,[1] K. A. Pimbblet[14] and M. Prescott[15]

[1]*Australian Astronomical Observatory, PO Box 915, North Ryde, NSW 1670, Australia*
[2]*Sydney Institute for Astronomy (SIfA), School of Physics, The University of Sydney, NSW 2006, Australia*
[3]*Research School of Astronomy & Astrophysics, The Australian National University, Cotter Road, Weston Creek, ACT 2611, Australia*
[4]*School of Physics, The University of Melbourne, Parkville, VIC 3010, Australia*
[5]*Astrophysics Research Institute, Liverpool John Moores University, Twelve Quays House, Egerton Wharf, Birkenhead CH41 1LD, UK*
[6]*European Southern Observatory, Karl-Schwarzschild-Str. 2, D-85748 Garching, Germany*
[7]*Institute for Computational Cosmology, Department of Physics, Durham University, South Road, Durham DH1 3LE, UK*
[8]*ICRAR, University of Western Australia, 35 Stirling Highway, Crawley, WA 6009, Australia*
[9]*SUPA, School of Physics and Astronomy, North Haugh, St Andrews, Fife KY16 9SS, UK*
[10]*European Southern Observatory, Alonso de Cordova 3107, Vitacura, Santiago, Chile*
[11]*Institut für Astro- und Teilchenphysik, Universität Innsbruck, Technikerstraβe 25, A-6020 Innsbruck, Austria*
[12]*Department of Physics and Astronomy, Macquarie University, NSW 2109, Australia*
[13]*Astronomy Centre, University of Sussex, Falmer, Brighton BN1 9QH, UK*
[14]*School of Physics, Monash University, Clayton, VIC 3800, Australia*
[15]*Department of Physics, University of the Western Cape, Private Bag X17, Bellville 7535, South Africa*

Accepted 2013 August 6. Received 2013 August 6; in original form 2013 January 8

ABSTRACT

We present observations of 18 galaxies from the Galaxy And Mass Assembly (GAMA) survey made with the SPIRAL optical integral field unit (IFU) on the Anglo-Australian Telescope. The galaxies are selected to have a narrow range in stellar mass ($6 \times 10^9 < M_* < 2 \times 10^{10}\,\mathrm{M}_\odot$) in order to focus on the effects of environment. Local galaxy environments are measured quantitatively using fifth nearest neighbour surface densities. We find that the total star formation rates (SFR) measured from the IFU data are consistent with total SFRs measured from aperture correcting either GAMA or Sloan Digital Sky Survey single-fibre observations. The mean differences are $\mathrm{SFR_{GAMA}/SFR_{IFU}} = 1.26 \pm 0.23$, $\sigma = 0.90$ and for the Sloan Digital Sky Survey we similarly find $\mathrm{SFR_{Brinchmann}/SFR_{IFU}} = 1.34 \pm 0.17$, $\sigma = 0.67$. Examining the relationships with environment, we find that off-centre and clumpy Hα emission is not significantly dependent on environment, being present in 2/7 (29^{+20}_{-11} per cent) galaxies in high-density environments (>0.77 Mpc^{-2}), and 5/11 (45^{+15}_{-13} per cent) galaxies in low-density environments (<0.77 Mpc^{-2}). We find a weak but not significant relationship of the total SFRs of star-forming galaxies with environment. Due to the size of our sample and the scatter observed we do not draw a definitive conclusion about a possible SFR dependence on environment. Examining the spatial distribution of the Hα emission, we find no evidence for a change in shape or amplitude of the radial profile of star-forming galaxies with environment. If these observations are borne out in larger samples, this would infer that any environment-driven star formation suppression must either act very rapidly (the 'infall-and-quench' model) or that galaxies must evolve in a density-dependent manner (an 'in situ evolution' model).

Key words: galaxies: clusters: general – galaxies: elliptical and lenticular, cD – galaxies: evolution – galaxies: kinematics and dynamics.

⋆ E-mail: sb@aao.gov.au

1 INTRODUCTION

The galaxy population we see today has some very distinctive features. One of the most fundamental is the separation of galaxies into a bimodal distribution according to colour (e.g. Strateva et al. 2001; Baldry et al. 2006). The colour largely relates to the age of the stars, with galaxies on the tight red sequence being mostly passive systems containing old stars. In contrast, the galaxies in the blue cloud generally show a younger stellar population (e.g. Taylor et al., in preparation). However, it is still unclear what drives this separation.

Recent research has focused on how blue star-forming galaxies can have their star formation quenched, moving them on to the red sequence. Red-sequence galaxies are preferentially found in denser environments (e.g. Blanton et al. 2005; Cooper et al. 2008; Thomas et al. 2010; Smith et al. 2012) and star formation is also clearly suppressed in those high-density environments (e.g. Lewis et al. 2002; Gómez et al. 2003; Kauffmann et al. 2004). This immediately suggests that environmental factors play an important role.

There is uncertainty, however, in how the change in star-forming properties as a function of environment manifests itself. Balogh et al. (2004) found that once luminosity is taken into account, the observed environmental difference is only due to the *fraction* of blue galaxies changing in each environment, rather than due to any change in the properties of the galaxy population. Star formation rates (SFRs) measured from single-fibre observations of the Hα emission line give similar conclusions: Peng et al. (2010) observed that the relationship between SFR and stellar mass was the same in the highest and lowest density environments. Recent results from the Galaxy And Mass Assembly (GAMA; Driver et al. 2011) survey also show that the fraction of star-forming galaxies falls with increasing environmental density (Wijesinghe et al. 2012; Robotham et al. 2013), but the SFR of the star-forming galaxies depends solely on their stellar mass, showing no change with their environment (Wijesinghe et al. 2012). These observations would imply that any mechanism that transforms galaxies in dense environments must be rapid or have happened a long time ago.

In contrast, research examining the strength of the 4000 Å break and the Balmer absorption lines (von der Linden et al. 2010) and ultraviolet (UV) imaging from the *Galaxy Evolution Explorer* (*GALEX*) space telescope (Rasmussen et al. 2012) suggests that both the star-forming fraction and the SFR in star-forming galaxies change as a function of environment, allowing for a longer timescale for any transformation.

The different conclusions drawn by these observations may have a number of causes, including the different ways that star formation and environment are measured, varying definition for star-forming galaxies and the inability of single-fibre observations to specify where that star formation is happening. This last point is crucial given that the proposed mechanisms for any modulation of star formation with environment can have very different spatial effects:

Ram-pressure stripping (Gunn & Gott 1972; Nichols & Bland-Hawthorn 2011), which can expel the gas from the disc, and *strangulation* (Larson, Tinsley & Caldwell 1980), which results when the gas is removed from the halo, should both preferentially remove gas in the outer parts of galaxies (e.g. Bekki 2009; Kapferer et al. 2009). These processes may be efficient at removing halo gas, which is observed in galaxy clusters (e.g. Sun, Donahue & Voit 2007; Randall et al. 2008). Ram-pressure stripping may also act in small and/or compact groups (McCarthy et al. 2008; Rasmussen et al. 2008) or on the outskirts of clusters (e.g. Merluzzi et al. 2013). The timescale of >2 Gyr for strangulation (McCarthy et al. 2008), however, seems to contradict the short time frame implied by observations. Although Prescott et al. (2011) find this to be the likely mechanism for the quenching of star formation in satellites hosted by isolated galaxies. Direct galaxy–galaxy interactions may also play a critical role in either triggering star formation (e.g. Moss & Whittle 1993; Ellison et al. 2008; Patton et al. 2013) or suppressing it, as seen in the less-massive galaxies of pairs when the pair mass ratio is large (Robotham et al. 2013).

Feedback from star formation in low-mass galaxies provides an internal mechanism for transformation. This provides a solution to the mismatch of the theoretical dark matter halo mass function and the observed stellar mass function (e.g. Baldry, Glazebrook & Driver 2008) by heating and/or expelling gas in haloes. Extreme outbursts of star formation may be triggered by mergers or interactions (e.g. Hopkins et al. 2009) even with very low luminosity galaxies or tidal debris (e.g. López-Sánchez 2010; Cluver et al. 2013), and frequently seen in isolated compact groups (e.g. López-Sánchez, Esteban & Rodríguez 2004; Konstantopoulos et al. 2010; Scudder, Ellison & Mendel 2012). This makes a link between internal and environmental effects. There is observational evidence of feedback from star formation (e.g. Veilleux, Cecil & Bland-Hawthorn 2005; Strickland & Heckman 2009; López-Sánchez et al. 2012).

At present it is still not clear which of the processes described above dominate in which situations. In one of the first attempts to study spatially resolved star formation in a very large sample as a function of a broad range of environment, Welikala et al. (2008, 2009) used galaxy colours to demonstrate that star formation is suppressed in the central parts of galaxies in high-density environments, apparently ruling out ram-pressure stripping as a significant influence in the general galaxy population.

While galaxy colours are a coarse measure of the integrated star formation history of a galaxy, the well-understood Hα emission line at 6563 Å probes near-instantaneous star formation (<10 Myr; e.g. Kennicutt 1998). Spatially resolved Hα measurements have only been made for samples of local galaxies either in the field or nearby clusters (e.g. Moss & Whittle 1993; Koopmann & Kenney 2004; Vogt et al. 2004; Fumagalli & Gavazzi 2008; Rose et al. 2010; Sánchez et al. 2012), often with narrow-band imaging, but have not been possible for a data set that covers a wide range in environment.

We present here observations of the spatially resolved Hα emission of galaxies over a wide range of environment from optical integral field unit (IFU) observations of galaxies selected from the GAMA survey. The primary goal of this paper is to measure the radial distribution of star formation and examine how that varies as a function of environment. We know that the SFRs of galaxies are strongly dependent on their stellar mass, but their dependence on environment is less clear. We therefore use GAMA to select a carefully controlled sample of galaxies with a narrow range of stellar masses ($M_* \sim 10^{10}\,\mathrm{M}_\odot$) in a range of environments. GAMA is highly spectroscopically complete (97 per cent; Driver et al. 2011), even in the densest regions. This is achieved by returning to each target area an average of 10 times, as described in Robotham et al. (2010). This enables accurate environment measurements including fifth nearest neighbour surface densities (e.g. Wijesinghe et al. 2012) and friends-of-friends group determination (Robotham et al. 2011).

We describe the selection of our sample in Section 2 and the observations in Section 3. In Section 4, we describe the method for measuring the emission line properties and then present the total SFRs and Hα surface brightness profiles of the sample in Sections 5 and 6. We discuss our findings in Section 7 before summarizing our conclusions in Section 8. Throughout this paper, we assume a Hubble constant of $H_0 = 70$ km s^{-1} Mpc^{-1} and $\Omega_\mathrm{M} = 0.3$, $\Omega_\Lambda = 0.7$.

Equivalent widths (EWs) for features in emission are quoted as positive numbers.

2 SAMPLE

We selected our sample from the GAMA (Driver et al. 2011[1]) survey which combines single-fibre spectroscopy (Hopkins et al. 2013) with a diverse set of supporting imaging data. We specifically selected galaxies from the first phase of the GAMA survey, referred to as GAMA I. There are ∼170 000 galaxies in the GAMA I sample down to $r = 19.4$ mag in two regions, each of 48 deg^2, and $r = 19.8$ mag in a third region, also of 48 deg^2. While the majority of the GAMA spectra have been obtained from the Anglo-Australian Telescope (AAT), the spectra and redshifts for brighter galaxies in these regions, like those targeted here, are obtained from the Sloan Digital Sky Survey (SDSS; York et al. 2000).

In order to focus specifically on the effects of environment rather than stellar mass we targeted galaxies with stellar masses $6 \times 10^9 < M_* < 2 \times 10^{10}\,\mathrm{M}_\odot$. The stellar mass measurements are from spectral energy distribution fits to optical broad-band photometry (Taylor et al. 2011) and have random uncertainties of ∼0.3 dex. Given the size of the uncertainties, no narrower window in stellar mass would be appropriate. We corrected the redshifts for the effects of peculiar velocity using the Tonry et al. (2000) multi-attractor flow model (z_{TONRY}; Baldry et al. 2012) and limited the sample to low redshifts, $0.02 < z_{\mathrm{TONRY}} < 0.06$, so that targets are close enough that we can spatially resolve them. This reduces the available sample to 688 galaxies. We are complete in stellar mass over the redshift range considered.

The nearest neighbour surface density, Σ_5, is calculated for all galaxies with reliable redshifts (nQ > 2; Driver et al. 2011). The fifth nearest neighbour metric is similar to the Σ_1 metric used in Brough et al. (2011). The surface density is defined using the projected comoving distance to the fifth nearest neighbour (d_5) with $\pm 1000\,\mathrm{km\,s^{-1}}$ within a pseudo-volume-limited density-defining population: $\Sigma_5 = 5/\pi d_5^2$. The density-defining population has absolute SDSS petrosian magnitudes $M_r < M_{r,\,\mathrm{limit}} - Qz$, k-corrected to $z = 0$ following Loveday et al. (2012), where $M_{r,\,\mathrm{limit}} = -20.0$ mag and Q defines the expected evolution of M_r as a function of redshift ($Q = 0.87$; Loveday et al. 2012). Densities are then corrected for the survey $r-$band redshift completeness as $\Sigma_5 = \Sigma_{5,\,\mathrm{raw}} \times 1/\mathrm{completeness}$. Galaxies where the nearest survey edge is closer than the fifth nearest neighbour have upper limits calculated and flags assigned. More details on this and other environment metrics available for GAMA will be provided in Brough et al. (in preparation).

There are 424 galaxies with stellar masses $6 \times 10^9 < M_* < 2 \times 10^{10}\,\mathrm{M}_\odot$ and $0.02 < z_{\mathrm{TONRY}} < 0.06$ that are not flagged as having been affected by a survey edge. These 424 galaxies have environmental densities $0.02 < \Sigma_5(\mathrm{Mpc}^{-2}) < 78$, with a median $\Sigma_5 = 0.77\,\mathrm{Mpc}^{-2}$. We randomly selected 18 galaxies across two density bins around the median density (<0.77 Mpc^{-2}; 11 galaxies and >0.77 Mpc^{-2}; 7 galaxies). The surface density distribution of the 424 possible targets and the 18 selected are illustrated in Fig. 1. The 18 targets selected have apparent SDSS petrosian magnitudes $m_r < 17.6$ mag and a mean effective semimajor axis radius, from two-dimensional (2D) Sérsic surface brightness fits to re-processed SDSS r-band imaging (Kelvin et al. 2012), of $R_{e,\,r} = 3.4$ arcsec. The properties of the 18 observed galaxies from the GAMA survey are described in Table 1.

[1] http://www.gama-survey.org

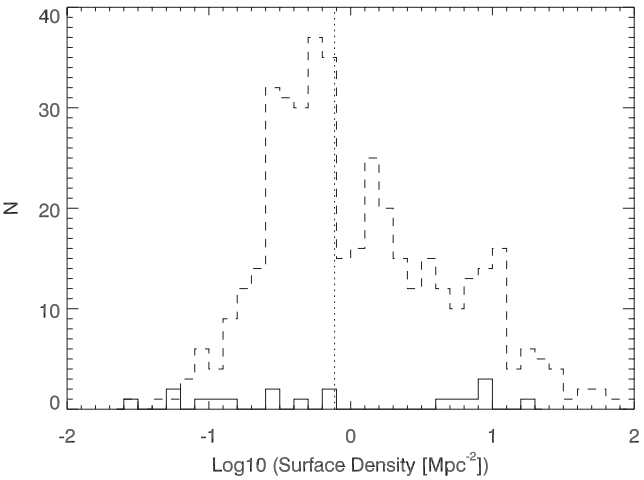

Figure 1. Histogram showing the surface density distributions of the 424 possible targets (dashed line) and the 18 observed galaxies (solid line). The dotted line indicates the median surface density of 0.77 Mpc^{-2} that divides the low- and high-density samples analysed here. The observed galaxies sample the possible density distribution well and the low- and high-density subsamples can be seen to be well separated.

We determined the effect the number of the nearest neighbour used has on the sample selected and the results presented here. We also calculated $\Sigma_{N=10}$ for the parent sample considered here (galaxies with stellar masses $6 \times 10^9 < M_* < 2 \times 10^{10}\,\mathrm{M}_\odot$ and $0.02 < z_{\mathrm{TONRY}} < 0.06$). The mean difference $\Sigma_{N=5} - \Sigma_{N=10} = 2.0 \pm 6.8\ \mathrm{Mpc}^{-1}$. The median $\Sigma_{N=10} = 0.95\ \mathrm{Mpc}^{-1}$, which does not move galaxies between the high- and low-density bins defined here. However, using $N = 10$ a large fraction of this sample (12 out of 18) are affected by survey edges, we therefore present all of our results using $N = 5$.

The GAMA groups catalogue (Robotham et al. 2011) is not volume limited so we cannot draw strong conclusions from the group properties of these galaxies. However, we do note that all galaxies in high-density environments are found in groups and that these generally have higher total dynamical masses ($7 \times 10^{12} < M_{\mathrm{dyn}} < 4 \times 10^{14}\,\mathrm{M}_\odot$) than the 3/11 galaxies in low-density environments that are found in pairs and groups ($7 \times 10^{11} < M_{\mathrm{dyn}} < 7 \times 10^{12}\,\mathrm{M}_\odot$). For information we also indicate in Table 1 whether the galaxies in groups are the central galaxy in their group (C), a satellite (S) or one of a pair of galaxies (P), where the group centre is defined following an iterative centre-of-light analysis (Robotham et al. 2011). None of these galaxies are at the centre of a group.

3 OBSERVATIONS

The data were taken in 2011 April, 2012 February and 2012 May with the SPIRAL IFU. SPIRAL is a 32 × 16 element rectangular microlens array coupled via an optical fibre feed to the dual-beam AAOmega spectrograph (Saunders, Cannon & Sutherland 2004; Sharp et al. 2006). It has a spatial sampling of 0.7arcsec spaxel^{-1} with no gaps, giving a field of view of 22.4 × 11.2 arcsec^2. We observed with the low-resolution 580V grating in the blue and the higher resolution 1000R grating in the red. These settings correspond to wavelength ranges of 3700–5700 Å and 6200–7300 Å and spectral resolutions of 1900 and 5000, respectively. Accounting for the sample redshift range, this targets the emission lines Hβ in the blue and Hα in the red. Observations were made during dark time,

Table 1. Properties of the observed sample of galaxies from GAMA (described in the text). The galaxies are divided into the two environmental density bins: high density (top of table) and low density (bottom of table).

GAMA ID	RA (J2000)	Dec. (J2000)	Stellar mass $\log(M_\odot)$	z_{TONRY}	Σ_5 (Mpc^{-2})	Group mass $\log(M_\odot)$	Central?	$R_{e,r}$ (arcsec)	Sérsic n_r
136624	11:43:17.06	−01:38:39.0	10.30	0.0463	16.33	13.8	S	2.24	2.4
220328	12:04:16.65	+01:32:46.5	9.83	0.0221	9.91	13.8	S	5.20	2.5
618152	14:18:05.49	+00:13:38.6	10.03	0.0543	8.25	14.6	S	3.56	0.9
227278	14:11:19.16	+01:18:34.3	10.13	0.0259	8.06	12.8	S	2.05	2.6
600916	09:12:06.92	+00:20:12.7	10.05	0.0549	7.71	12.9	S	5.50	1.1
136880	11:45:20.90	-01:48:46.1	9.78	0.028	6.04	13.8	S	3.79	1.6
600978	09:12:45.34	+00:20:24.9	9.91	0.0549	4.89	12.9	S	5.08	0.8
422359	08:42:13.17	+02:37:28.6	10.10	0.051	0.71	–		2.47	1.6
106252	14:21:05.39	+00:51:54.3	9.83	0.0550	0.65	–		2.34	0.6
227962	14:22:01.09	+01:11:50.3	9.88	0.0558	0.42	12.8	S	2.02	0.9
92770	14:30:14.98	+00:37:17.0	9.87	0.0271	0.31	–		3.28	1.2
418448	09:04:50.24	+02:30:23.3	10.02	0.0557	0.26	–		2.03	2.5
375909	08:45:32.05	+01:17:36.0	9.96	0.0450	0.14	12.9	P	4.23	0.8
536005	12:00:00.48	−01:01:40.7	10.09	0.0483	0.12	–		2.62	1.4
535319	11:49:15.69	−00:58:36.9	9.89	0.0606	0.09	11.9	P	4.08	0.8
55150	12:03:01.01	−00:17:28.2	10.09	0.0417	0.06	–		4.47	0.7
371177	08:41:39.24	+00:58:26.7	10.03	0.0608	0.06	–		2.63	1.7
583637	11:43:17.98	−00:10:53.8	10.01	0.0577	0.03	–		3.28	1.2

with an average seeing of 1.5 arcsec (FWHM). Each galaxy was observed for 3 × 2400 s with individual observations dithered by 1–2 spaxels in right ascension and declination in order to avoid four isolated dead elements in SPIRAL. Spectrophotometric standard stars were also observed each night, in order to prepare a sensitivity function.

Initial data reduction, from raw detector output to dark-subtracted, bias-subtracted, wavelength-calibrated, sky-subtracted, 1D-extracted spectra, was achieved using the 2DFDR pipeline (Croom, Saunders & Heald 2004). The root-mean-square dispersion around the wavelength solution is 0.12 Å in the blue and 0.03 Å in the red spectra. The dispersion around the 5577 Å sky line is 0.09 Å. Twilight flat-field frames were also observed in order to account for relative fibre-to-fibre transmission variations. As none of our targets completely fill the SPIRAL field of view, a sky background spectrum was calculated by taking the median over pixels without galaxy light. The final data analysis was carried out using custom IDL routines. The sensitivity function determined from comparing the total observed flux from spectrophotometric standard stars to that predicted as a function of wavelength was applied. The final flux calibration was done by applying SDSS *g*- and *i*-band fibre magnitudes (measured in the 3 arcsec SDSS fibre) to the blue and red SPIRAL spectra integrated over a 3-arcsec aperture respectively for each galaxy. The calculated offset was then applied to the individual SPIRAL spectra. Comparison with the flux-calibrated SDSS spectra indicates a 6 per cent uncertainty in the flux calibration level of the blue spectra (covering the Hβ line) and 10 per cent in the red spectra (covering the Hα line). Following flux calibration individual frames were aligned and mosaicked using telescope offset information. Frames are scaled based on a comparison of overlap regions in the mosaic, to account for minor variations in transparency and seeing.

4 EMISSION-LINE MEASURES

In order to examine the radial distribution of star formation, high signal-to-noise ratio spectra were produced by combining spectra within annuli for each galaxy. Each annulus is defined as a radial de-projection of the galaxy, based on position angle and inclination information derived from GAMA analysis of SDSS imaging data (Kelvin et al. 2012). Prior to stacking, each spectrum from individual spaxels is velocity matched based on a velocity fields derived from emission and absorption fits to a block-averaged (3 × 3 spaxel) data cube. The [N II], Hα and [N II] region is fitted with a four-component model, three emission lines and Hα absorption, assuming common velocities and widths for the emission components and with the ratio of the flux of the nitrogen lines fixed at 3.28. The emission redshift is allowed to float with respect to that of the absorption line. Errors are estimated from a quadrature summation of the statistic values returned for the best-fitting model and the parameter distribution from a bootstrap resampling of each composite spectrum.

Individual Gaussian fits to the Hα and Hβ emission lines in each spaxel of each SPIRAL data cube were also made for examination purposes. The resulting Hα flux and velocity maps as well as SDSS thumbnail images for the same field of view are shown for each galaxy in Appendix A. The maps are presented in order of environmental density (highest density environment first). There are some interesting features in the Hα flux maps including off-centre (600978, 92770, 371177) and clumpy emission (618152, 535319, 55150, 583637). Gerssen, Wilman & Christensen (2012) also observe clumpy emission in their VIMOS IFU observations of SDSS galaxies. Two of the off-centre and clumpy emission features are in galaxies in high-density environments (618152 and 600978; 29^{+20}_{-11} per cent), while the remaining five are in galaxies in the low-density environments (45^{+15}_{-13} per cent). We conclude that off-centre and clumpy Hα emission does not significantly depend on environment in our data.

The Hα velocity maps (Appendix A) show that all galaxies with strong Hα emission show ordered rotation in that emission line, even when the emission is clumpy or off-centre. This is consistent with observations at higher redshifts showing that clumpy galaxies are well fitted by ordered disc models (e.g. Wisnioski et al. 2011).

5 STAR FORMATION RATES

We first examine the total SFRs of the galaxies. The total SFR measurements are made by summing the obscuration-corrected Hα

Table 2. Spectral measurements from IFU observations and the GAMA survey. Total Hα fluxes and obscuration-corrected star formation rates (SFR) are given for the IFU observations. The GAMA measurements (described in the text) are made from SDSS stellar absorption-corrected single-fibre spectra. The column 'Class' details whether a galaxy is classified as an AGN by GAMA and whether it would be classified as star forming (SF) or non-star forming (NSF) by Wijesinghe et al. (2012). The galaxies are divided into the two environmental density bins: high density (top of table) and low density (bottom of table). Galaxy 220328 only shows Hα in absorption and Galaxies 136880 and 227278 are active galactic nuclei (AGN).

GAMA ID	$f_{H\alpha,IFU}$ ($\times 10^{-17}$ erg s^{-1} cm^{-2})	SFR_{IFU} ($M_\odot$ yr^{-1})	Hβ EW_{SDSS} (Å)	BD_{GAMA}	SFR_{GAMA} ($M_\odot$ yr^{-1})	Class
136624	266	0.02	0.10	1.50	0.01	NSF
220328	–	–	−0.08	2.42	0.01	NSF
618152	618	0.79	4.21	4.57	1.58	SF
227278	85	–	0.66	3.37	–	AGN
600916	276	0.35	1.46	5.09	0.79	NSF
136880	44	–	0.10	5.22	–	AGN
600978	1608	1.92	6.92	3.96	2.14	SF
422359	1328	1.62	6.10	4.32	2.13	SF
106252	165	0.19	3.23	5.13	0.64	SF
227962	1930	2.36	8.38	3.61	1.87	SF
92770	366	0.07	0.69	3.07	0.04	NSF
418448	793	1.03	4.19	3.62	0.88	SF
375909	2976	4.04	8.43	4.85	5.09	SF
536005	2140	1.68	8.76	4.57	4.11	SF
535319	1425	2.04	6.42	3.75	1.72	SF
55150	5630	5.89	5.91	4.27	4.26	SF
371177	730	1.37	3.00	3.41	0.56	SF
583637	958	1.42	2.18	4.04	0.65	NSF

flux ($f_{H\alpha}$ [erg s^{-1} cm^{-2}]) over the observed extent of the galaxy. The flux is obscuration corrected using the Balmer decrement (BD; Hα flux/Hβ flux) measured in individual spaxels. The Hα luminosity is then

$$L_{H\alpha}(W) = 4\pi d_L^2 f_{H\alpha}(BD/2.86)^{2.36}, \quad (1)$$

where d_L is the luminosity distance in centimetres. The BD is a unitless obscuration sensitive parameter and its departure from the Case B recombination value of 2.86 indicates dust attenuation along the line of sight. While dust geometries are complex, this approach implicitly models the dust as a foreground screen averaged over the galaxy (Calzetti 2001). The exponent in the dust obscuration correction factor is equal to $k(\lambda_{H\alpha})/[k(\lambda_{H\beta}) - k(\lambda_{H\alpha})]$, and $k(\lambda)$ at a given λ is determined from the Cardelli, Clayton & Mathis (1989) Galactic dust extinction curve (derived from observations of the UV extinction of stars). This is found to well describe the obscuration of the ionized gas in star-forming galaxies (Calzetti 2001; Gunawardhana et al. 2011). The SFRs are then calculated using the relationship given by Kennicutt (1998) assuming a Salpeter (1955) initial mass function (IMF), i.e. $SFR = L_{H\alpha}(W)/1.27 \times 10^{34}$. These values are given in Table 2.

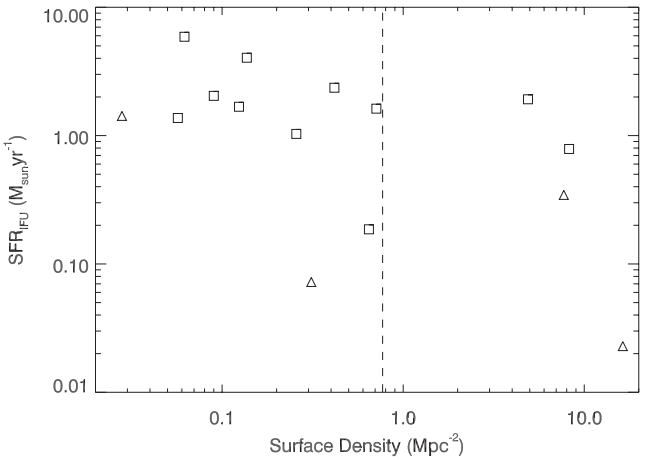

Figure 2. Total star formation rates of the star-forming galaxies as a function of environmental density. The dashed line indicates the median surface density of 0.77 Mpc^{-2} that divides the low- and high-density subsamples analysed here. There is a weak correlation between log10(SFR_{IFU}) and log10(Σ_5), significant only at the 1.8σ level. We indicate which galaxies would have been classified by Wijesinghe et al. (2012) as star forming (squares) and non-star forming (triangles); some of those classified as non-star forming are still forming stars.

5.1 Dependence on environment

We compare the total SFRs of the star-forming galaxies (SFR_{IFU}) with their environmental density in the top panel of Fig. 2. We note that the only absorption-dominated galaxy (galaxy 220328) in this sample is found in the highest density environment. The observed mean SFR_{IFU} (low density) = 1.97 ± 0.51 is more than a factor of 2 higher than that at high density (= 0.77 ± 0.42). To determine the significance of an environmental dependence we apply a Kolmogorov–Smirnov two sample test to the SFRs in the low- and high-density environments. This gives a probability of 19.6 per cent that the two samples are drawn from the same parent population. A Spearman rank correlation of the relationship between log10(Σ_5) and log10(SFR) shows that the correlation between these parameters is only significant at the 1.8σ level.

Given the small size of our sample and the scatter observed we examine whether we can detect a significant relationship with environment. We tested this by adjusting the mean SFRs of the galaxies in the high-density environments while maintaining their standard deviation and re-ran our statistical tests. A weakly significant

correlation between environment and SFR is observed (at a 2.3σ level) if the mean SFRs in high-density environments are a factor of 5 lower than those in the low-density environments (a factor of 2 lower than observed).

We observe a weak but not significant relationship of SFR with environment in this sample. Due to the small sample size and observed scatter we cannot draw a strong conclusion about a universal SFR dependence, or lack of, on environment.

5.2 Comparison with Wijesinghe et al. (2012)

We use the total SFR measurements made from our IFU observations to analyse the Wijesinghe et al. (2012) star-forming galaxy classification. They define star-forming galaxies as those not classified as active galactic nuclei (AGN) using the Kewley et al. (2001) definition with non-absorption corrected Hβ EW > 1.5 Å, BD < 15 and SFR $> 10^{-3}\,M_{\odot}\ yr^{-1}$. We use the single-fibre GAMA measurements to determine whether our sample would meet their star-forming classification.

GAMA utilizes the MPA/JHU emission-line catalogue[2] to obtain absorption-corrected line fluxes and EWs for these bright galaxies. These line measurements are made from stellar absorption-corrected SDSS spectra. The GAMA SFRs are calculated as described in Hopkins et al. (2013) and Gunawardhana et al. (2013) and are given in Table 2. In summary, the Hα luminosity is calculated from the Hα EW, which is aperture corrected and extinction corrected using the BD as per the IFU measurements. The GAMA SFRs are then calculated using the Kennicutt (1998) relationship. We note that dust obscuration is not excessive in any of the galaxies in this sample: their mean BDs are 3.9 ± 0.9 (Table 2) which translates to a dust obscuration factor of $\sim$2.

Wijesinghe et al. (2012) do not correct Hβ EWs for stellar absorption for the definition of their star-forming sample; however, they do correct Hα EWs by adding a constant correction of 0.7 Å. We therefore use that addition here, i.e. stellar absorption corrected Hβ EW > 2.2 Å, to determine whether our sample would meet their star-forming classification. Table 2 shows that two of the galaxies in this sample are classified as AGN from the single-fibre analysis and five do not make the Wijesinghe et al. (2012) star-forming classification, based on their Hβ EW. Fig. 2 shows that four of these 'non-star forming' galaxies are still forming stars at some level. These galaxies are a clear indication of the need to take care when separating galaxies into distinct star-forming and non-star-forming populations.

5.3 Aperture corrections

Calculating the total SFR of galaxies from single-fibre observations requires a correction for the portion of the galaxy enclosed by the size of the fibre used: an aperture correction. In the GAMA survey the total SFR is calculated by aperture correcting the Hα flux measured within the fibre following the method of Hopkins et al. (2003). This aperture correction relies on the assumption that the line emission scales directly with the stellar continuum, as measured by the r-band magnitude. However, there is obviously some uncertainty in that assumption. We use the total SFR measurements made from our IFU observations to analyse this correction further. The IFU SFRs are compared to the GAMA SFR in the top panel of Fig. 3.

[2] http://www.mpa-garching.mpg.de/SDSS/DR7/

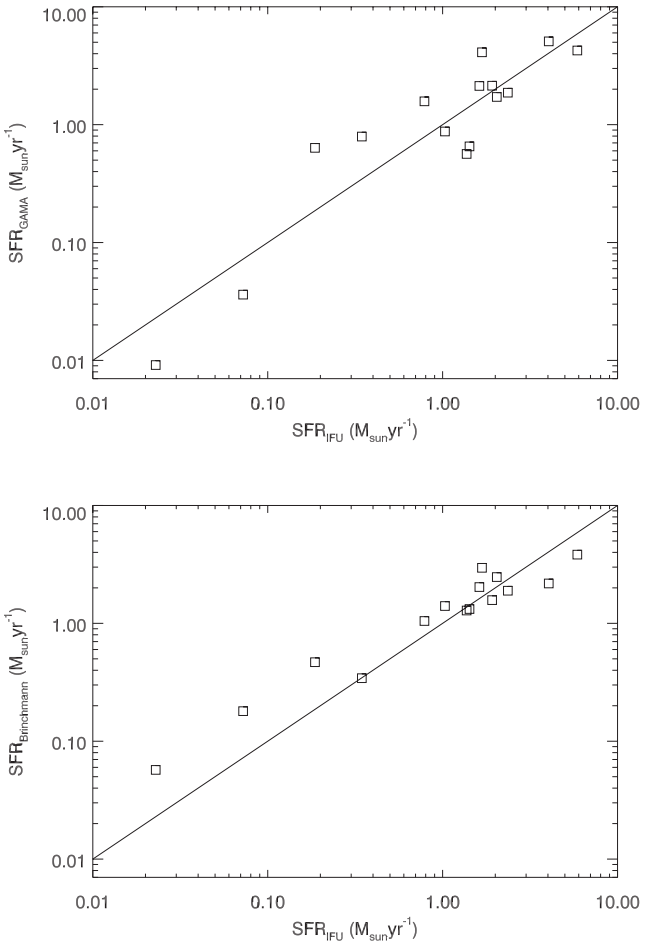

Figure 3. Comparing total star formation rates from IFU and single-fibre observations of the star-forming galaxies. The solid lines indicate the 1:1 relationships. The top panel shows the comparison between the total IFU star formation rates and the total aperture-corrected GAMA single-fibre star formation rates. The mean ratio is $SFR_{GAMA}/SFR_{IFU} = 1.26 \pm 0.23$. The bottom panel shows the comparison between the total IFU star formation rates and the total SDSS single-fibre SFR aperture-corrected as per Brinchmann et al. (2004). The mean ratio $SFR_{Brinchmann}/SFR_{IFU} = 1.34 \pm 0.17$. The aperture-corrected SFRs are in relatively good agreement with those from the IFU measurements, no matter which aperture correction method is used. However, the uncertainties can still be large for individual systems.

We do not include either galaxy 220328 or the two AGN in this analysis due to a lack of observable star formation and AGN contamination, respectively. The mean difference $SFR_{GAMA}/SFR_{IFU} = 1.26 \pm 0.23$, $\sigma = 0.90$, i.e. SFR_{GAMA} is on average 26 per cent higher than SFR_{IFU} with a broad dispersion (the standard error on the mean is calculated as $\sigma/\sqrt{N}$).

Gerssen et al. (2012) analysed the aperture correction applied to calculate total SFR from SDSS spectra by Brinchmann et al. (2004) using IFU observations of 24 star-forming (Hα EW > 20 Å, $f_{H\alpha} > 448 \times 10^{-17}$ erg s^{-1} cm^{-2}), low-mass ($1 \times 10^8 < M_* < 3 \times 10^{10}\,M_{\odot}$) SDSS galaxies. They found the Brinchmann et al. (2004) aperture corrections to underestimate the total SFR by a factor of 2.5 with a dispersion of 1.75, significantly larger than the factor of 1.26 difference and 0.90 dispersion we find between our IFU SFR and the GAMA aperture-corrected SFRs. We analyse whether the GAMA aperture correction is significantly different to that used by Brinchmann et al. (2004) by also comparing

SFR_{IFU} with the most recent total SFR estimated by Brinchmann for the SDSS data release seven (DR7)[3] in the bottom panel of Fig. 3.

Brinchmann et al. (2004) determine total SFRs using a Bayesian approach to calculate the likelihood of fits of the observed spectrum to Charlot & Longhetti (2001) models, which incorporate an obscuration model. They note that, to first approximation, the dust corrections are based on the Hα/Hβ ratio. The Brinchmann et al. (2004) total SFRs are calculated with a Kroupa (2001) IMF and we convert to the Salpeter (1955) IMF used here by multiplying their measurements by 1.5. They aperture correct in an empirical manner using the distribution of the SFR/M* ratio at a given $(g-r, r-i)$ colour and the photometry outside the fibre to correct the fibre SFR. This aperture correction is updated for the DR7 by calculating the light outside the fibre for each galaxy, and then fitting stochastic models to the photometry.

We find a mean difference $SFR_{Brinchmann}/SFR_{IFU} = 1.34 \pm 0.17$, $\sigma = 0.67$, i.e. we also find that the Brinchmann correction overestimates the SFR. This is a much smaller difference than Gerssen et al. (2012) found. This also suggests a marginal trend towards higher SFR estimates by aperture correcting using either method, although again with a high dispersion. These results suggest that contrary to the claim by Gerssen et al. (2012), the aperture-corrected SFRs for these low-mass galaxies are in relatively good agreement with those estimated from the IFU measurements, no matter which method is used. The large dispersion does however mean that the uncertainties can still be large for individual systems. In addition, this is still only a small sample, and reliable statistics on total SFR estimates compared to those from aperture-corrected measurements will need a much larger sample.

6 RADIAL Hα PROFILES

We determine whether any dependence of SFR on environment is evident in the spatial distributions of Hα emission in these galaxies. The Hα surface brightness is calculated by dividing the summed flux in each elliptical annulus by the area of the annulus. These radial profiles are shown in Fig. 4.

Fig. 4 shows that the radial Hα surface brightness profiles of galaxies in both environments (solid and dashed lines) are very similar to one another, being centrally concentrated with high surface brightnesses over all radii studied. In contrast, the surface brightness profiles of the galaxies with no emission above the detection limit of 2×10^{18} erg s^{-1} cm^{-2} arcsec^{-2} (dotted lines) are only present in the highest density environments. Of these, galaxy 220328 is dominated by absorption and the 2 AGN (136880, 227278) show central emission (dot–dashed lines) and no significant emission beyond that.

We further analyse the relationship of the profiles of the star-forming galaxies with their environment with straight-line fits to the Hα surface brightness profiles taking into account the uncertainties in the Hα flux measurements. We do not include the three galaxies with undetected emission in this analysis. We show the fitted gradient and intercept values and 1σ errors of the 15 star-forming galaxies as a function of environment in Fig. 5.

We test the correspondence between these parameters with a Spearman rank correlation, finding that the gradients are correlated with $\log10(\Sigma_5)$ at a significance of only 0.25σ and the intercepts are correlated at a significance of 0.4σ. There is no dependence of the radial distribution of the Hα emission as a function of environment.

[3] These are the total values given in gal_totsfr_dr7_v5_2.fits available at: http://www.mpa-garching.mpg.de/SDSS/DR7/sfrs.html.

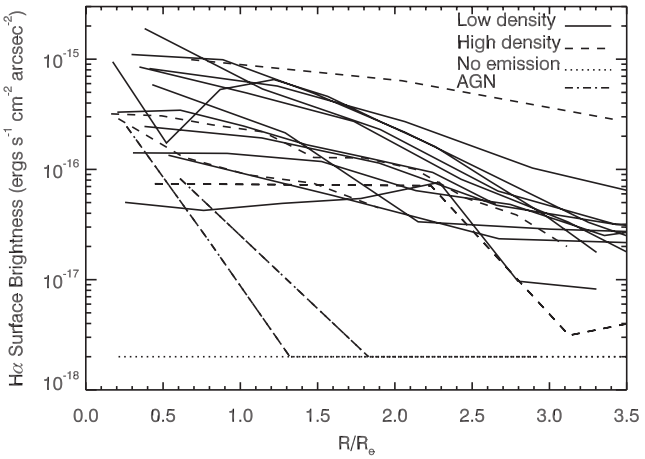

Figure 4. Radial Hα surface brightness profiles as a function of the effective radius of the galaxy. Solid lines show galaxies in low-density environments (<0.77 Mpc^{-2}) and dashed lines show galaxies in high-density environments (>0.77 Mpc^{-2}), dotted lines indicate regions that do not show emission above the detection limit of 2×10^{18} erg s^{-1} cm^{-2} arcsec^{-2} and dot–dashed lines indicate the emission of the two AGN. The average seeing approximates to $R/R_e \sim 0.2$. The profiles do not show a dependence on environment.

The galaxies observed here all have very similar stellar masses and we are observing no significant dependence in either Hα surface brightness profile shape or amplitude of the star-forming galaxies as a function of environment.

7 DISCUSSION

We have presented observations of the spatially resolved Hα emission of galaxies over a wide range of environment with the aim of examining how the radial distribution of star formation varies as a function of environment. We observe a weak but not significant difference in total SFR and no difference of radial profile of the star-forming galaxies' Hα emission as a function of local galaxy environment in this sample of 18 galaxies with stellar masses $\sim 10^{10}\,M_\odot$.

Before making general comments on the effect of environment on star formation based on our observations, we show that our sample is unbiased and representative of the broader galaxy population in this narrow stellar mass range. The uncertainties given below are 1σ binomial errors (Cameron 2011). There are 424 galaxies in GAMA with accurate surface densities (i.e. not affected by survey edges) that have stellar masses, $6 \times 10^9 < M_* < 2 \times 10^{10}\,M_\odot$, and redshifts, $0.02 < z_{TONRY} < 0.06$. We use an updated version of the Wijesinghe et al. (2012) classification (those not classified as AGN with stellar absorption-corrected Hβ EW > 1.0 Å, BD < 15 and SFR $>10^{-3}\,M_\odot$ yr^{-1}) to define star-forming galaxies. Of the 424 galaxies, there are roughly equal numbers of AGN in each environmental density: 21/212 (10^{+2}_{-2} per cent) in low-density environments and 19/212 (9^{+2}_{-2} per cent) in high-density environments. There are 147/212 (69^{+3}_{-3} per cent) of galaxies in low-density environments that would make our star-forming galaxy criteria and 93/212 (44^{+3}_{-3} per cent) in high-density environments.

In the sample observed here, in the low-density environments, there are no AGN and 11/11 (100_{-14} per cent) of the galaxies make the updated star-forming galaxy criteria. In the high-density

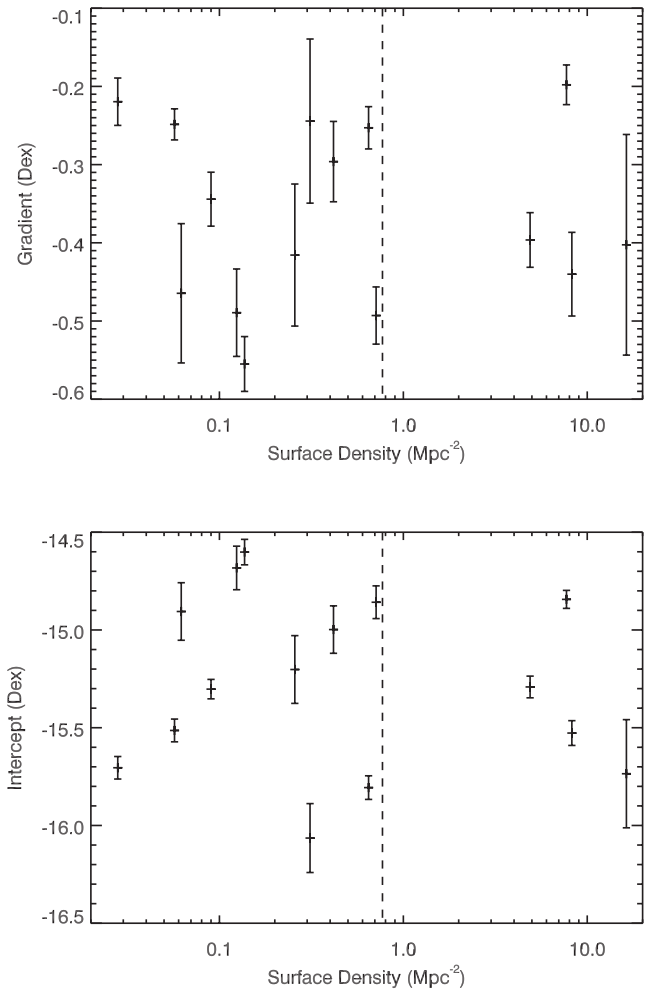

Figure 5. Parameters of straight-line fits to Hα surface brightness profiles of the star-forming galaxies as a function of environmental density. The top panel shows the gradient of the fits. The gradients are correlated with environment at a significance of only 0.25σ. The bottom panel shows the fitted intercept. The intercepts are correlated with environment at a significance of 0.4σ. The error bars show the 1σ uncertainties on the profile fits. The fits to the surface brightness profiles do not show a dependence on environment.

environment there are 2/7 (29^{+20}_{-11} per cent) AGN and a further 2/7 non-star-forming galaxies, meaning that 3/7 (43^{+18}_{-15} per cent) make our updated star-forming galaxy criteria.

We can conclude from this that the numbers of galaxies in this sample meeting the star-forming criteria in each environment are within 2.2σ of those in the broader sample. This sample therefore follows the distributions of the general population.

The sample studied here is broadly representative of the general population and we find that the total SFRs of the star-forming galaxies do not depend significantly on their local environmental density (Fig. 2). However, due to the small size of the sample and the scatter observed we do not draw a definitive conclusion about a possible SFR dependence on environment. Examining the spatial information provided by the Hα surface brightness profiles, we observe no difference in amplitude or shape of the Hα surface brightness profile of star-forming galaxies as a function of environment (Figs 4 and 5). We also find no evidence for 'clumpiness' in Hα emission depending on environment (Appendix A).

The only comparable analysis to date examined the spatial star formation histories inferred from the colours of 44 964 galaxies in SDSS (Welikala et al. 2008). They found that the mean SFR of each galaxy as a function of radius is dominated by star formation in the central regions of galaxies, and that the trend for suppression in high-density environments is driven by a reduction in that central star formation. They also find that the mean SFR in the outskirts is independent of environmental effects. Welikala et al. (2008) conclude that the environment itself cannot suppress the star formation as the outer regions should otherwise be most affected and therefore this points to an evolutionary or AGN feedback origin. We do not observe any significant radial dependence of the surface brightness of Hα emission as a function of environment, either centrally or in the outer regions. However, the suppression observed by Welikala et al. (2008) in their highest star-forming galaxies (SFR $> 1.02\,\mathrm{M}_{\odot}\ \mathrm{yr}^{-1}$) is a factor of <2, of the order SFR $\sim 0.002\,\mathrm{M}_{\odot}\ \mathrm{yr}^{-1}$. This difference is significantly smaller than we can detect with these observations so we cannot rule out the suppression they observe. Welikala et al. (2009) considered the density–morphology relation in the same sample, observing the strongest relation in the lowest luminosity galaxies with the highest SFRs. However, they conclude that it cannot solely explain the observed suppression of star formation in galaxies in high-density environments. Table 1 shows that three out of the four galaxies with Sérsic $n_r > 2$ are in high-density environments, of which two are not star forming. The mean n (high density) $= 1.7 \pm 0.3$ and (low density) $= 1.2 \pm 0.2$, suggesting that there are signs of a difference in morphology as a function of environment in our sample but that it alone does not explain the lack of significant dependence of star formation on environment.

If these observations are borne out in larger samples, then combined with the known decreasing fraction of star-forming galaxies as a function of increasing environmental density (e.g. Balogh et al. 2004; Baldry et al. 2006; Bolzonella et al. 2010; McGee et al. 2011; Wetzel, Tinker & Conroy 2012; Wijesinghe et al. 2012) and the small numbers of galaxies in transition between star forming and non-star forming observed in large samples (e.g. Wijesinghe et al. 2012; Mendel et al. 2013), this would suggest that if environment does drive the change in fractional contribution it must either act very rapidly (the 'infall-and-quench' model; e.g. Balogh et al. 2004; Bamford et al. 2008; Nichols & Bland-Hawthorn 2011; Wetzel et al. 2013) or have occurred a long time ago due to density-dependent evolution (an 'in situ evolution' model; Wijesinghe et al. 2012), such that galaxies in transition are rare at this time. In situ evolution would involve galaxies in dense environments evolving faster than galaxies in low-density environments, building their stellar mass faster and earlier, leading to the observed morphology–density relation, and consistent with the measured SFR–density relations at both low and high redshift. The in situ evolution model is similar to 'downsizing' (Cowie et al. 1996), 'staged evolution' (Noeske et al. 2007) and the 'mass quenching' model of Peng et al. (2010); however, galaxies of common mass would evolve differently in different environments in order to give rise to the observed population mix. Transition redshifts, at which the dependence of the specific SFRs of galaxies on increasing environmental density transitions from increasing to decreasing, have been observed (e.g. Elbaz et al. 2007; Greene et al. 2012) giving weight to this argument.

We note that there are some caveats to this argument. First, this is a small sample. A larger sample would increase the robustness of our results. Our sample also does not reach the densest cluster environments where galaxies are observed to be affected by ram pressure stripping (Owers et al. 2012; Merluzzi et al. 2013) and tidal distortions (e.g. Moss & Whittle 1993; Vogt et al. 2004; Bretherton, Moss & James 2013). Our choice of environmental metric may

play a role as the SFRs of galaxies at a fixed stellar mass have been observed to increase as a function of increasing cluster-centric radius, rather than environmental density (von der Linden et al. 2010; Rasmussen et al. 2012; Haines et al. 2013). In addition, van den Bosch et al. (2008) argue that the relationship between SFR and environment is driven by evolutionary differences between central and satellite galaxies in a dark matter halo and we are only studying satellite galaxies here. We will examine the effects of our choice of environmental metric in a forthcoming paper (Brough et al., in preparation). Dust may also play a role as Koyama et al. (2013) find dustier galaxies in higher-density environments mask a trend of increasing specific SFR with increasing environmental density.

To separate the two scenarios of 'infall-and-quench' and 'in situ evolution' and address these caveats requires observations of a very large sample of galaxies, covering a broad range of stellar mass and environment, in order to place stringent limits on the number density of any transition galaxies. It will be crucial to detect the very faintest levels of star formation present, as well as its spatial dependence. This will require very high signal-to-noise ratio IFU spectra to enable careful decomposition of emission and absorption contributions (Sarzi et al. 2006). The new Sydney Australian Astronomical Observatory (AAO) Multi-object-IFU (SAMI; Croom et al. 2012) instrument with 13 deployable IFUs over a 1° field of view, and associated survey will enable this crucial next step.

8 CONCLUSIONS

We present observations of the spatially resolved star formation as a function of local environment from optical IFU observations of 18 galaxies with stellar masses $M_* \sim 10^{10}\,\mathrm{M}_\odot$ selected from the GAMA survey. Our conclusions can be summarized as follows.

(i) The total SFRs measured from the IFU data are consistent with the total aperture-corrected SFRs measured from both the GAMA and SDSS surveys. The mean differences are $\mathrm{SFR_{GAMA}/SFR_{IFU}} = 1.26 \pm 0.23$, $\sigma = 0.90$; $\mathrm{SFR_{Brinchmann}/SFR_{IFU}} = 1.34 \pm 0.17$, $\sigma = 0.67$.

(ii) Off-centre and clumpy Hα emission does not depend on environment. It is present in 2/7 (29^{+20}_{-11} per cent) galaxies in high-density environments and 5/11 (45^{+15}_{-13} per cent) galaxies in low-density environments show similar features.

(iii) In this sample, we see weak but not significant evidence of a dependence of total SFR on environment, using IFU observations for the first time.

(iv) We observe no clear environmental trend on the amplitude or shape of the radial profile of Hα emission. This implies that, for this sample, there is no strong outside-in or inside-out quenching.

(v) The lack of dependence of the radial profile of Hα emission shape or amplitude on environment suggests that if environment drives the known change in fractional contribution of star-forming galaxies in different environments, it must either act very rapidly (the 'infall-and-quench' model) or galaxies must evolve in a density-dependent manner (an 'in situ evolution' model), to explain the lack of transition galaxies observed in large samples.

In order to identify more precisely how and when any transition due to environment occurs requires high signal-to-noise ratio, spatially resolved spectra as well as a very large sample that covers a range in stellar mass, environment and star formation stage, including post-starburst galaxies. The new Sydney Australian Astronomical Observatory (AAO) Multi-object-IFU (SAMI; Croom et al. 2012) instrument will address this with its associated survey.

ACKNOWLEDGEMENTS

We thank the anonymous referee for their comments which greatly improved the paper. SC acknowledges the support of the Australian Research Council via a Future Fellowship (FT100100457). GAMA is a joint European–Australasian project based around a spectroscopic campaign using the Anglo-Australian Telescope. The GAMA input catalogue is based on data taken from the Sloan Digital Sky Survey and the UKIRT Infrared Deep Sky Survey. Complementary imaging of the GAMA regions is being obtained by a number of independent survey programmes including *GALEX* MIS, VST KIDS, VISTA VIKING, *WISE*, *Herschel*-ATLAS, GMRT and ASKAP providing UV to radio coverage. GAMA is funded by the STFC (UK), the ARC (Australia), the AAO and the participating institutions. The GAMA website is http://www.gama-survey.org.

REFERENCES

Baldry I. K., Balogh M. L., Bower R. G., Glazebrook K., Nichol R. C., Bamford S. P., Budavari T., 2006, MNRAS, 373, 469
Baldry I. K. et al., 2012, MNRAS, 421, 621
Baldry I. K., Glazebrook K., Driver S. P., 2008, MNRAS, 388, 945
Balogh M. L., Baldry I. K., Nichol R., Miller C., Bower R., Glazebrook K., 2004, ApJ, 615, L101
Bamford S. P., Rojas A. L., Nichol R. C., Miller C. J., Wasserman L., Genovese C. R., Freeman P. E., 2008, MNRAS, 391, 607
Bekki K., 2009, MNRAS, 399, 2221
Blanton M. R., Lupton R. H., Schlegel D. J., Strauss M. A., Brinkmann J., Fukugita M., Loveday J., 2005, ApJ, 631, 208
Bolzonella M. et al., 2010, A&A, 524, A76
Bretherton C. F., Moss C., James P. A., 2013, A&A, 553, A67
Brinchmann J., Charlot S., White S. D. M., Tremonti C., Kauffmann G., Heckman T., Brinkmann J., 2004, MNRAS, 351, 1151
Brough S. et al., 2011, MNRAS, 413, 1236
Calzetti D., 2001, PASP, 113, 1449
Cameron E., 2011, Publ. Astron. Soc. Aust., 28, 128
Cardelli J. A., Clayton G. C., Mathis J. S., 1989, ApJ, 345, 245
Charlot S., Longhetti M., 2001, MNRAS, 323, 887
Cluver M. E. et al., 2013, ApJ, 765, 93
Cooper M. C. et al., 2008, MNRAS, 383, 1058
Cowie L. L., Songaila A., Hu E. M., Cohen J. G., 1996, AJ, 112, 839
Croom S., Saunders W., Heald R., 2004, Anglo-Australian Observatory Epping Newsletter, 106, 12
Croom S. M. et al., 2012, MNRAS, 421, 872
Driver S. P. et al., 2011, MNRAS, 413, 971
Elbaz D. et al., 2007, A&A, 468, 33
Ellison S. L., Patton D. R., Simard L., McConnachie A. W., 2008, AJ, 135, 1877
Fumagalli M., Gavazzi G., 2008, A&A, 490, 571
Gerssen J., Wilman D. J., Christensen L., 2012, MNRAS, 420, 197
Gómez P. L. et al., 2003, ApJ, 584, 210
Greene C. R. et al., 2012, MNRAS, 425, 1738
Gunawardhana M. L. P. et al., 2011, MNRAS, 415, 1647
Gunawardhana M. L. P. et al., 2013, MNRAS, 433, 2764
Gunn J. E., Gott J. R., III, 1972, ApJ, 176, 1
Haines C. P. et al., 2013, arXiv:e-prints
Hopkins A. M. et al., 2003, ApJ, 599, 971
Hopkins A. M. et al., 2013, MNRAS, 430, 2047
Hopkins P. F. et al., 2009, MNRAS, 397, 802
Kapferer W., Sluka C., Schindler S., Ferrari C., Ziegler B., 2009, A&A, 499, 87
Kauffmann G., White S. D. M., Heckman T. M., Ménard B., Brinchmann J., Charlot S., Tremonti C., Brinkmann J., 2004, MNRAS, 353, 713
Kelvin L. S. et al., 2012, MNRAS, 421, 1007
Kennicutt R. C., Jr, 1998, ARA&A, 36, 189

Kewley L. J., Dopita M. A., Sutherland R. S., Heisler C. A., Trevena J., 2001, ApJ, 556, 121
Konstantopoulos I. S. et al., 2010, ApJ, 723, 197
Koopmann R. A., Kenney J. D. P., 2004, ApJ, 613, 851
Koyama Y. et al., 2013, MNRAS, 434, 423
Kroupa P., 2001, MNRAS, 322, 231
Larson R. B., Tinsley B. M., Caldwell C. N., 1980, ApJ, 237, 692
Lewis I. et al., 2002, MNRAS, 334, 673
López-Sánchez Á. R., 2010, A&A, 521, A63
López-Sánchez Á. R., Esteban C., Rodríguez M., 2004, ApJS, 153, 243
López-Sánchez Á. R., Koribalski B. S., van Eymeren J., Esteban C., Kirby E., Jerjen H., Lonsdale N., 2012, MNRAS, 419, 1051
Loveday J. et al., 2012, MNRAS, 420, 1239
McCarthy I. G., Frenk C. S., Font A. S., Lacey C. G., Bower R. G., Mitchell N. L., Balogh M. L., Theuns T., 2008, MNRAS, 383, 593
McGee S. L., Balogh M. L., Wilman D. J., Bower R. G., Mulchaey J. S., Parker L. C., Oemler A., 2011, MNRAS, 413, 996
Mendel J. T., Simard L., Ellison S. L., Patton D. R., 2013, MNRAS, 429, 2212
Merluzzi P. et al., 2013, MNRAS, 429, 1747
Meurer G. R. et al., 2006, ApJS, 165, 307
Moss C., Whittle M., 1993, ApJ, 407, L17
Nichols M., Bland-Hawthorn J., 2011, ApJ, 732, 17
Noeske K. G. et al., 2007, ApJ, 660, L43
Owers M. S., Couch W. J., Nulsen P. E. J., Randall S. W., 2012, ApJ, 750, L23
Patton D. R., Torrey P., Ellison S. L., Mendel J. T., Scudder J. M., 2013, MNRAS, 433, L59
Peng Y.-J. et al., 2010, ApJ, 721, 193
Prescott M. et al., 2011, MNRAS, 417, 1374
Randall S., Nulsen P., Forman W. R., Jones C., Machacek M., Murray S. S., Maughan B., 2008, ApJ, 688, 208
Rasmussen J., Mulchaey J. S., Bai L., Ponman T. J., Raychaudhury S., Dariush A., 2012, ApJ, 757, 122
Rasmussen J., Ponman T. J., Verdes-Montenegro L., Yun M. S., Borthakur S., 2008, MNRAS, 388, 1245
Robotham A. et al., 2010, Publ. Astron. Soc. Aust., 27, 76
Robotham A. S. G. et al., 2011, MNRAS, 416, 2640
Robotham A. S. G. et al., 2013, MNRAS, 416, 2640
Rose J. A., Robertson P., Miner J., Levy L., 2010, AJ, 139, 765
Salpeter E. E., 1955, ApJ, 121, 161
Sánchez S. F. et al., 2012, A&A, 538, A8
Sarzi M. et al., 2006, MNRAS, 366, 1151
Saunders W., Cannon R., Sutherland W., 2004, Anglo-Australian Observatory Epping Newsletter, 106, 16
Scudder J. M., Ellison S. L., Mendel J. T., 2012, MNRAS, 423, 2690
Sharp R. et al., 2006, Proc. SPIE, 6269, 14
Smith R. J., Lucey J. R., Price J., Hudson M. J., Phillipps S., 2012, MNRAS, 419, 3167
Strateva I. et al., 2001, AJ, 122, 1861
Strickland D. K., Heckman T. M., 2009, ApJ, 697, 2030
Sun M., Donahue M., Voit G. M., 2007, ApJ, 671, 190
Taylor E. N. et al., 2011, MNRAS, 418, 1587
Thomas D., Maraston C., Schawinski K., Sarzi M., Silk J., 2010, MNRAS, 404, 1775
Tonry J. L., Blakeslee J. P., Ajhar E. A., Dressler A., 2000, ApJ, 530, 625
van den Bosch F. C., Aquino D., Yang X., Mo H. J., Pasquali A., McIntosh D. H., Weinmann S. M., Kang X., 2008, MNRAS, 387, 79
Veilleux S., Cecil G., Bland-Hawthorn J., 2005, ARA&A, 43, 769
Vogt N. P., Haynes M. P., Giovanelli R., Herter T., 2004, AJ, 127, 3300
von der Linden A., Wild V., Kauffmann G., White S. D. M., Weinmann S., 2010, MNRAS, 404, 1231
Welikala N., Connolly A. J., Hopkins A. M., Scranton R., 2009, ApJ, 701, 994
Welikala N., Connolly A. J., Hopkins A. M., Scranton R., Conti A., 2008, ApJ, 677, 970
Wetzel A. R., Tinker J. L., Conroy C., 2012, MNRAS, 424, 232
Wetzel A. R., Tinker J. L., Conroy C., van den Bosch F. C., 2013, MNRAS, 432, 336
Wijesinghe D. B. et al., 2012, MNRAS, 423, 3679
Wisnioski E. et al., 2011, MNRAS, 417, 2601
York D. G. et al., 2000, AJ, 120, 1579

APPENDIX A: Hα EMISSION-LINE MAPS

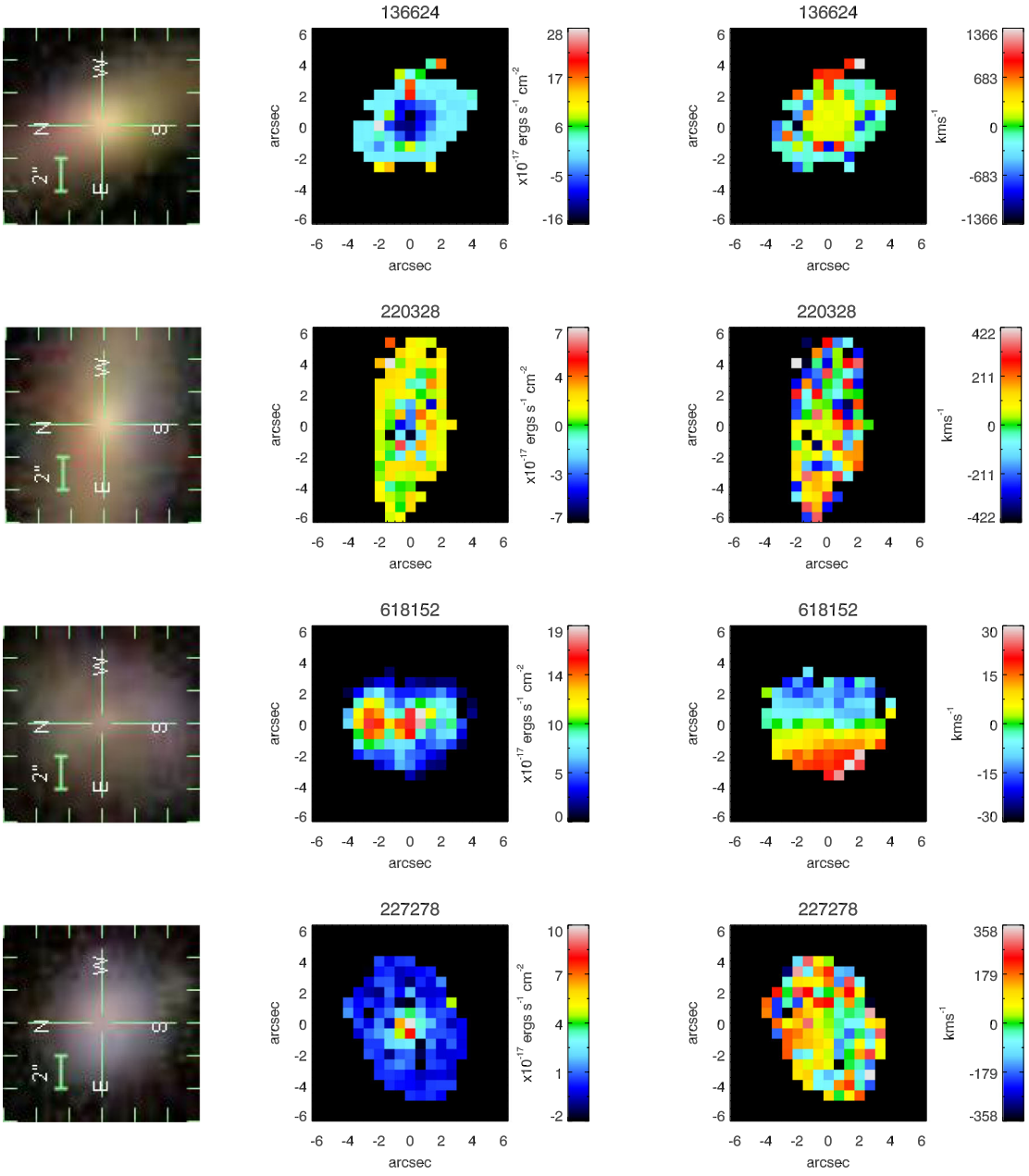

Figure A1. High-density environment galaxy sample. From left to right: SDSS thumbnail image of SPIRAL field of view, Hα flux map of central region; Hα velocity map of central region. Only spaxels with signal-to-noise ratios >3 are shown.

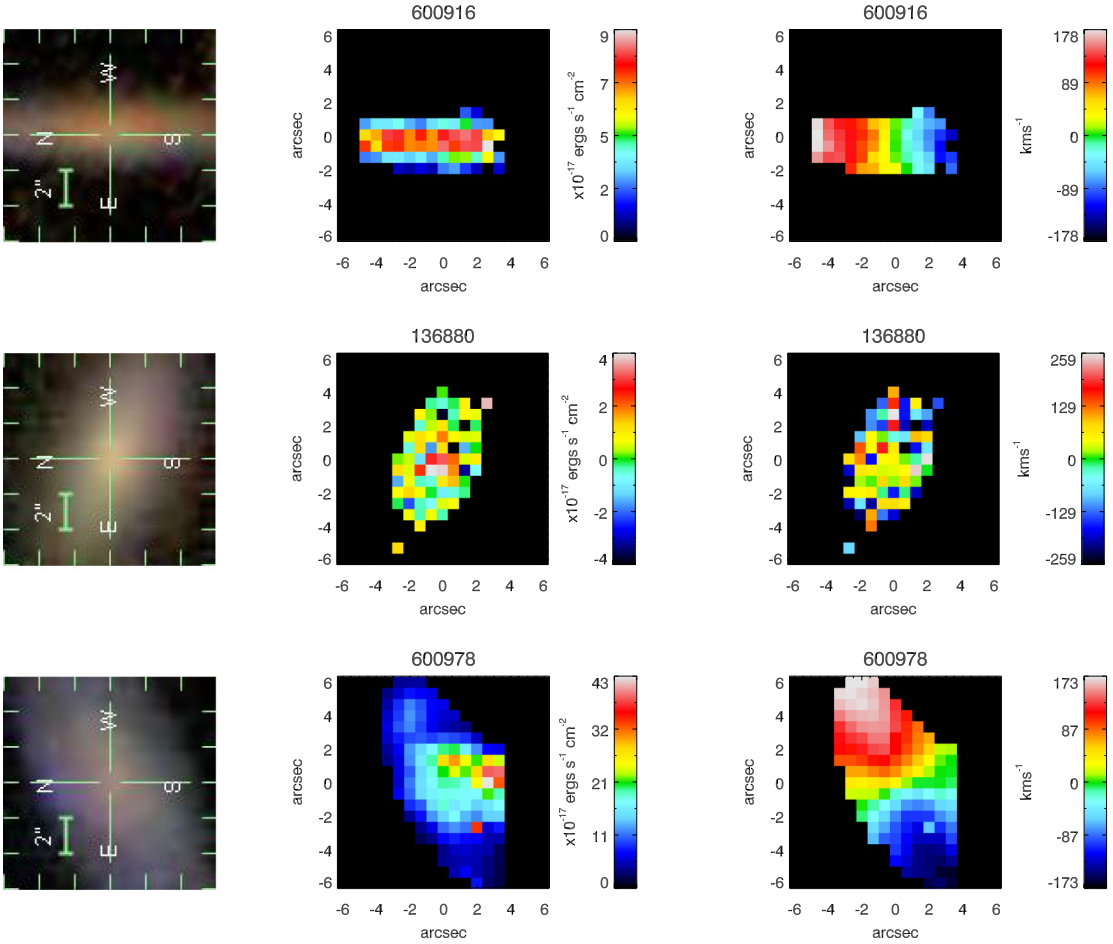

Figure A2. High-density environment galaxy sample – cont. From left to right: SDSS thumbnail image of SPIRAL field of view, Hα flux map of central region; Hα velocity map of central region. Only spaxels with signal-to-noise ratios >3 are shown.

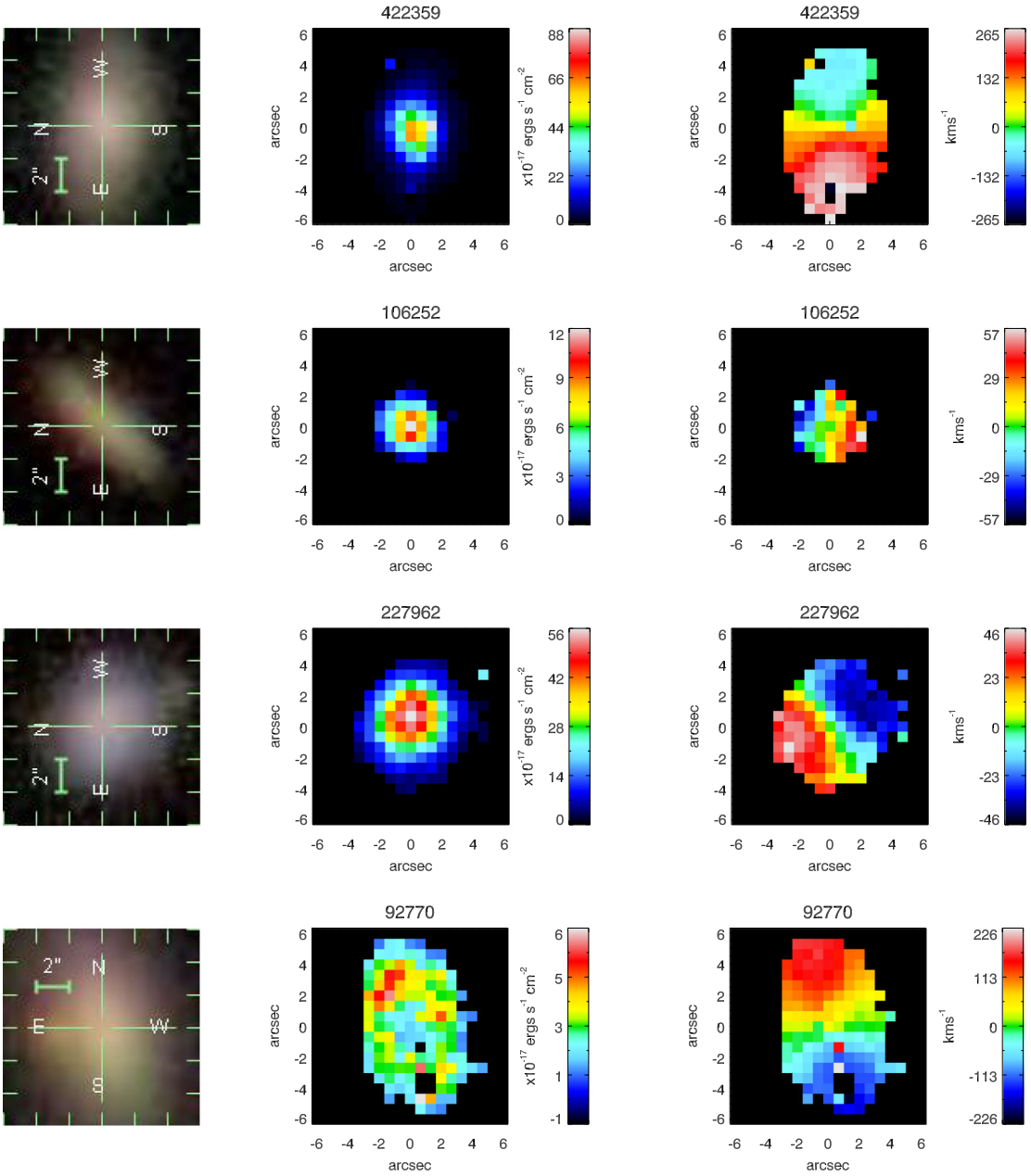

Figure A3. Low-density environment galaxy sample. From left to right: SDSS thumbnail image of SPIRAL field of view, Hα flux map of central region; Hα velocity map of central region. Only spaxels with signal-to-noise ratios >3 are shown.

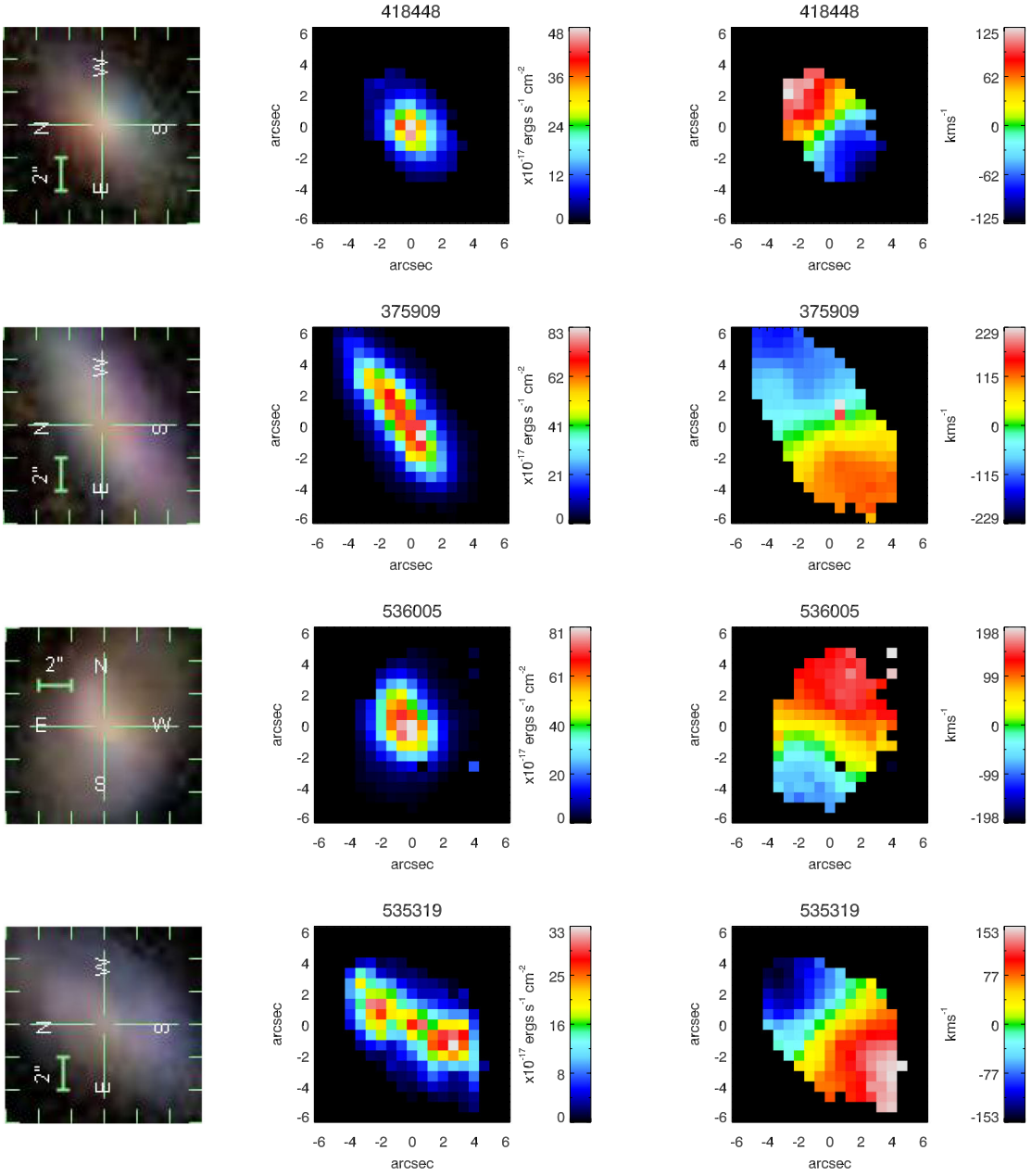

Figure A4. Low-density environment galaxy sample cont. From left to right: SDSS thumbnail image of SPIRAL field of view, Hα flux map of central region; Hα velocity map of central region. Only spaxels with signal-to-noise ratios >3 are shown.

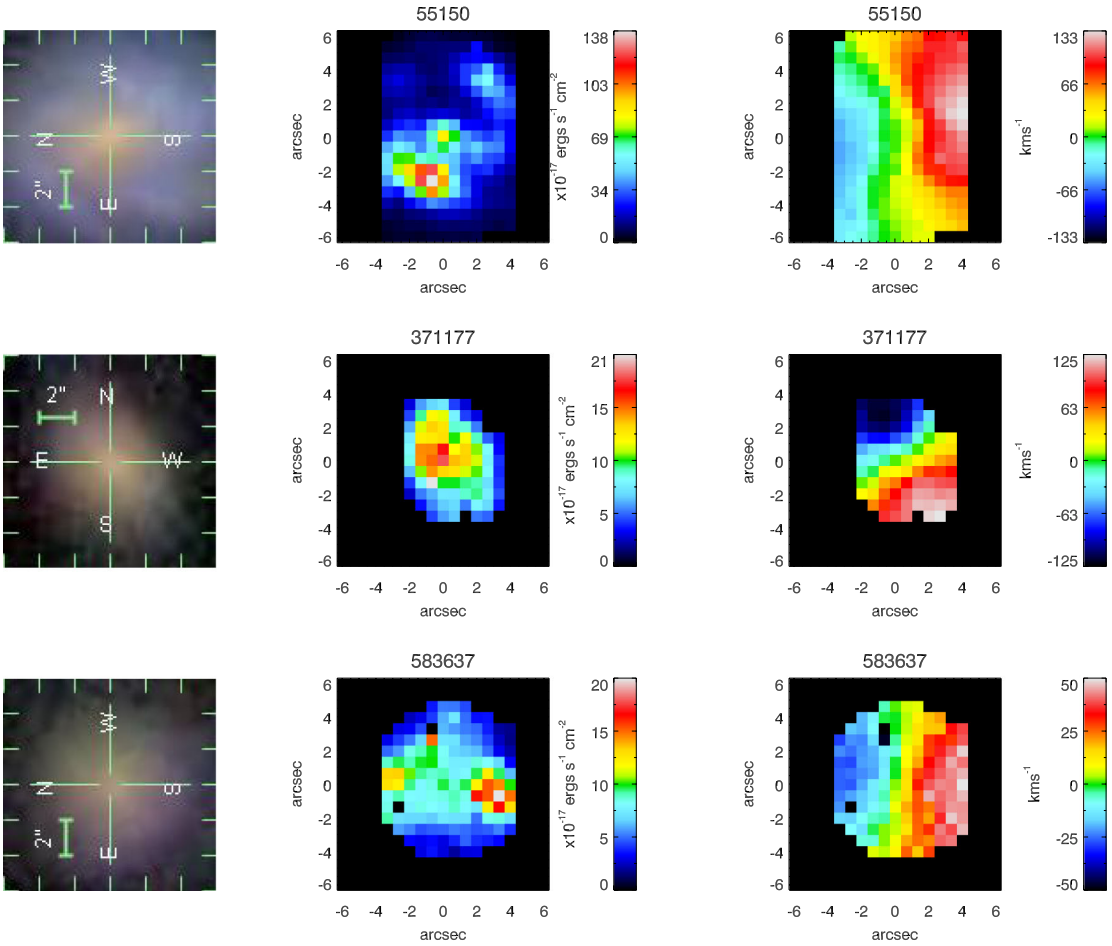

Figure A5. Low-density environment galaxy sample cont. From left to right: SDSS thumbnail image of SPIRAL field of view, Hα flux map of central region; Hα velocity map of central region. Only spaxels with signal-to-noise ratios >3 are shown.

This paper has been typeset from a TEX/LATEX file prepared by the author.